Biology of Reproduction, 2024, **110(5)**, 924–935
https://doi.org/10.1093/biolre/ioae015
Advance access publication date 25 January 2024
Research Article

Activation of interleukin 33-NFκB axis in granulosa cells during atresia and its role in disposal of atretic follicles†

Jean Wu, Colin Carlock, Kiana Tatum, Junbo Shim, Cindy Zhou and Yahuan Lou*

Department of Diagnostic Sciences, The University of Texas Health Science Center at Houston, Houston, TX, USA
***Correspondence:** Department of Diagnostic and Biomedical Sciences, The University of Texas HSC at Houston, 5326 Behavioral and Biomedical Science Building (BBSB), 1941 East Road, Houston, TX 77054, USA. Tel: +17134864059; E-mail: yahuan.lou@uth.tmc.edu

†**Grant Support:** This work was supported by NIH grant R01 HD049613 and partially by R01 DK077857 and R21 AG067311 (YL).

Abstract

It has been previously shown that the cytokine interleukin 33 is required for two processes, i.e., autophagic digestion of granulosa cells and recruitment of macrophages into atretic follicles, for full disposal of atretic follicles. Now, this study shows that activation of interleukin 33-suppression of tumorigenicity 2–Nuclear Factor κB (NFκB) axis in granulosa in early atretic follicles may regulate those two events. Injection of human chorionic gonadotropin has been shown to induce a transient peak of interleukin 33 expression with synchronized atresia. In this model, interleukin 33-independent expression of suppression of tumorigenicity 2 in granulosa cells was detected in early atretic follicles before macrophage invasion. The activation of NFκB pathway in ovaries was further demonstrated *in vivo* in Tg mice with luciferase-reporter for NFκB activation; the activation was microscopically localized to granulosa cells in early atretic follicles. Importantly, antibody blockage of interleukin 33 or interleukin 33 Knock-out (KO) (*Il33*$^{-/-}$) not only inhibited NFκB activity in ovaries, but it also altered expression of two key genes, i.e., reduction in proinflammatory interleukin6 (IL6) expression, and a surge of potential autophagy-inhibitory mammalian target of rapamycin (mTOR) expression in atretic follicles. By contrast, apoptosis and other genes, such as interleukin1β (IL1β) were not affected. In conclusion, in parallel to apoptosis, atresia signals also trigger activation of the interleukin 33-suppression of tumorigenicity 2–NFκB pathway in granulosa, which leads to (1) down-regulated expression of mTOR that is a negative regulator of autophagy and (2) up-regulated expression of proinflammatory IL6.

Summary Sentence
Interleukin 33–suppression of tumorigenicity 2–NFκB axis is activated in granulosa cells of early atretic follicles to downregulate mTOR, which, in turn, intensifies autophagic digestion of atretic follicles for self-disposal.

Graphical Abstract

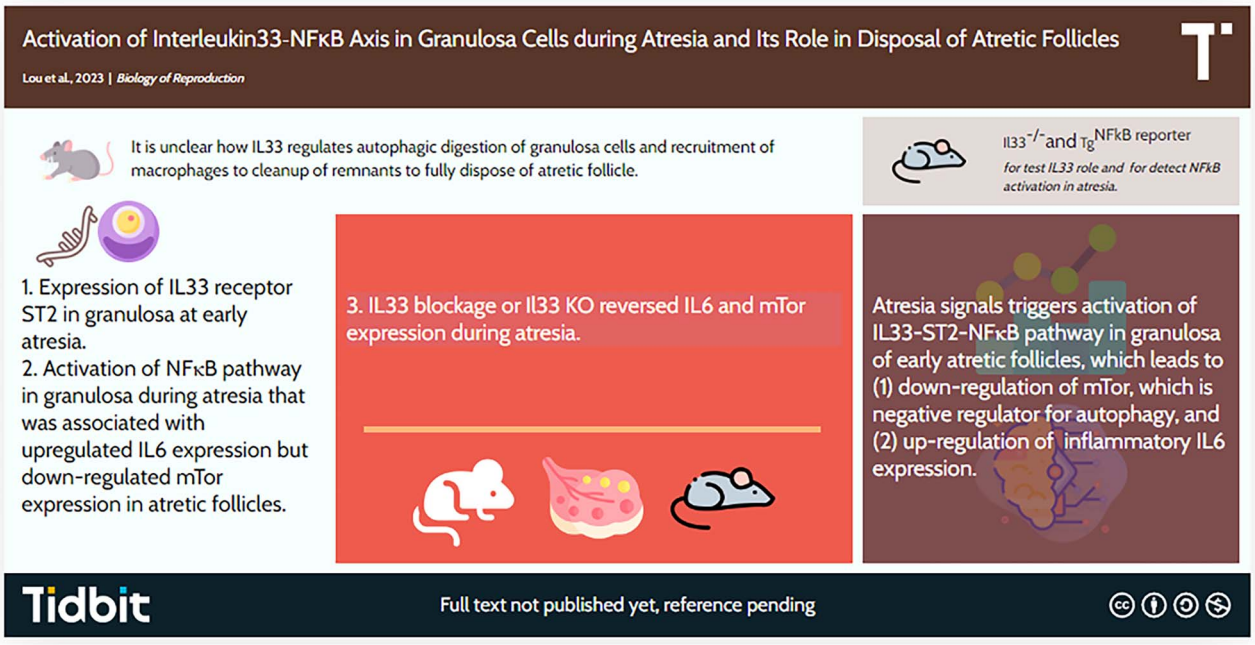

Key words: IL33, ST2, NFκB, granulosa, atresia, tissue disposal

Received: January 13, 2023. **Revised:** May 22, 2023. **Accepted:** January 18, 2024

Introduction

Follicular atresia is a complex, hormonally controlled process that is initiated with apoptosis in oocytes and granulosa cells [1]. Oocytes develop within ovarian follicles, but the majority will be eliminated through atresia, with only one dominant follicle selected for ovulation in mono-ovulatory species, or a cohort in poly-ovulatory species. It is important to fully dispose of those dying and unnecessary follicles. Autophagy allows elimination of a large number of cells in a process involving extensive tissue destruction [2], and its involvement in disposal of atretic follicles has been suggested [3–7]. A previous study has demonstrated that autophagy is a major mechanism for disposal of atretic follicles in parallel to apoptosis in mice [8]. This was achieved by observing an increase LC3II/LC3I ratio and autophagosomes within the granulosa cells of early atretic follicles. LC3 (microtubule-associated proteins 1A/1B light chain 3B) is a central protein in the autophagy pathway with two forms LC3I and LC3II. The transformation of LC3I to LC3II is critical for the formation of autophagosomes, and thus, an increase LC3II/LC3I ratio is a reliable measurement for autophagy activity [9]. This observation was further corroborated by the direct detection of the unique, two-layer structure of autophagosomes within the cytoplasm of granulosa cells in atretic follicles using electron microscopy [8, 10]. Involvement of autophagy in atresia was also reported by a recent study in rats [11]. In addition, a previous study has also detected two subsets of macrophages, i.e., IA/IE$^+$ and CD68$^+$ that invade atretic follicles at early and after middle stage, respectively, possibly to clean up the remnants from autophagic digestion [8, 12].

Our previous study has determined that cytokine interleukin 33 (IL33) is critical for the above two events, i.e., autophagy and macrophage invasion for disposal of atretic follicles. IL33 is a member of the IL1 cytokine family [13]. It is first stored in the nuclei, and a cytokine domain of 20kd is released after cleavage [14]. Protein suppression of tumorigenicity 2 (ST2) pairs with IL1-receptor-accessary-protein (IL1RAP, a common co-receptor for all IL1 cytokines) to form the receptor for IL33, which triggers the NFκB transcription pathway [15]. Beyond its roles in immune regulation, previous studies have shown its unique role in tissue homeostasis [8, 16–18]. Through comparison between *WT* and *Il33*$^{-/-}$ mice, it was demonstrated that IL33 orchestrates the two processes for full disposal of atretic follicles. Thus, *Il33*$^{-/-}$ ovaries show a lack of autophagy in granulosa cells and absence of macrophages in atretic follicles [8]. Although apoptosis occurs normally in *Il33*$^{-/-}$ ovaries, atretic follicles collapse, leading to accumulation of massive disintegrated cells and tissues, which produce lipofuscins and other reactive oxidative species (ROS). Those toxic substances, in turn, diffuse into surrounding normal follicles. Consequently, *Il33*$^{-/-}$ female mice show significantly shrunken oocyte reservoirs at their reproductive peak, and have a greatly shortened reproductive life [8]. It was concluded that IL33 is critical for the above two events, i.e., autophagy and macrophage invasion for disposal of atretic follicles.

This study is designed to further elucidate how IL33 regulates autophagy and macrophage invasion during atresia, with a focus on activation of the IL33–ST2-NFkB axis in atretic follicles. First, it is important to note, regulation of autophagy is mainly through cellular protein modification or signal transduction pathways, e.g., mTOR, but less dependent on up-regulation of expression of autophagy related genes, such as *Atgs* [19–21]. mTOR is particular interesting, as it is not only a potential regulator for autophagy, but also cross-talks with the NFκB pathway [22–27]. Secondly, a previous study has shown a surge of IL33 expression in ovaries post-equine chorionic gonadotropin (eCG)/human chorionic gonadotropin (hCG) treatment, which is associated with a wave of atresia after 13 h [16]. Another study has revealed silencing of NFκB activity in ovulating follicles, and thus, NFκB activity after hCG injection was unlikely related to ovulation [28]. Treatment of hCG associated surge of IL33 provides an opportunity to examine the IL33–ST2–NFκB axis and its possible roles in atresia. Third, apoptosis is well recognized as the first sign of atresia. It has been shown that the invasion of IA/IE$^+$ macrophages into atretic follicles shortly after apoptosis. Thus, apoptosis and IA/IE$^+$ macrophage invasion are used as markers to distinguish those early atretic follicles for examination of the NFκB pathway.

Materials and methods

Mice and their treatment

The C57BL/6 (B6) mice were purchased from Harlan (Indianapolis, IN, USA). *Il33*$^{\text{tm1(KOMP)Vlcg}}$ (*Il33*$^{-/-}$) mice were created from ES cell clone 12663E-H2 (Regeneron Pharmaceuticals, Rensselaer, NY, USA) and introduced into live mice by the KOMP Repository and the Mouse Biology Program (www.mousebiology.org) at the University of California Davis. *Il33*$^{-/-}$ and their *Il33*$^{+/-}$ and *WT* littermates were identified through genotyping as described previously [8]. *Tg*$^{(NFkB\text{-}RE\text{-}Luc)}$ mice, which carry a transgene containing six NFκB-responsive elements (RE) from the CMVα (immediate early) promoter placed upstream of a basal SV40 promoter, and a modified firefly luciferase cDNA, were obtained from Taconic BioSciences (Rensselaer, NY, USA). The mice were maintained in the animal facility at The University of Texas Health Science Center at Houston and allowed to acclimate for a minimum of 7 days. All animal procedures in this study were approved by the institutional animal welfare committee. Ovaries were harvested and fixed in 2% paraformaldehyde or snap-frozen in liquid nitrogen. In some cases, ovaries were used for isolation of total RNA (Ambion, Austin TX, USA). For eCG/hCG injection, the animals were injected with eCG (Sigma, St. Louis, MO, USA) at 5 IU/mouse intraperitoneally (i.p.), followed by i.p. injection of hCG, 5 IU/mouse (Sigma, St. Louis, MO, USA) 48 h later. Mice were sampled at 9 h or at designated times. For injection of neutralizing IL33 antibody (rat monoclonal antibody, R&D), each mouse (8 weeks old) was injected through a tail i.v. at a dose of 0.1 mg/mouse 24 h before eCG/hCG treatment [20]. A control group of mice were injected with rat IgG as isotype controls.

Whole body scanning and microscopic localization of luciferase-mediated bioluminescence

The *Tg*$^{(NFkB\text{-}RE\text{-}Luc)}$ female mice (8–10 weeks) were treated by eCG/hCG, or randomly selected. Four age-matched male *Tg*$^{(NFkB\text{-}RE\text{-}Luc)}$ mice and three B6 female mice were used as controls. Mice were i.p. injected with D-luciferin (10 μg/g bodyweight, PerkinElmer, Waltham, MA, USA). Mice were scanned by IVIS® Spectrum In Vivo Imaging System

(PerkinElmer) for the whole-body luminescent density 10–15 min after injection. In a separate experiment, five treated $Tg^{(NFkB\text{-}RE\text{-}Luc)}$ female mice were euthanized at 9 h after hCG injection, and their ovaries snap frozen in liquid nitrogen. Ten micrometer frozen sections were cut for microscopic detection of luminescence. Briefly, after mounting on slides, 10 μL of D-luciferin from a Luciferase Assay System kit (Promega, Madison, WI, USA) was added to the section and equilibrated for 2 min according to manufacturer's protocol; the slide was then sealed with a 0.1 mm space between slide and cover. Selected areas of the section were first imaged (phase contrast image, x200), followed by luminescence image exposure in darkness for 30 s. In some cases, the sections were stained by multi-color immunofluorescence using antibody to luciferase in combination with anti-ZP3 antibody.

Antibodies

The antibodies from BD Biosciences (San Jose, CA, USA) include biotin labeled anti-mouse IA/IE (rat IgG2a, 2G9) and Alexa-488-labeled anti-mouse F4/80 (rat IgG2a, BM8). Allophycocyanin (APC)-labeled anti-mouse ST2 mAb were obtained from Biolegend (San Diego, CA, USA). Biotinylated anti-mouse IL33 antibody and rat anti-mouse IL33 mAb (neutralizing) were from R&D System (Minneapolis, MN, USA) or ProSci (Charleston, SC, USA). Goat anti-luciferase polyclonal antibody was from ThermoFisher (Waltham, MA, USA), and purified anti-ZP3 (IE-10) mAb from Sigma-Aldrich (St. Louis, MO, USA). Secondary reagents Alexa-555, Alexa-594 and Alexa-647-labeled (Life Technologies, Carlsbad, CA, USA) and PE labeled (BD Biosciences) streptavidin were used to visualize biotin labeled Abs. Biotin/avidin and anti-mouse CD16/32 mAb (D34-485, BD Biosciences) were used for blocking non-specific binding. Various immunoglobulin isotypes used as negative controls were from BD Biosciences.

Immunofluorescence and quantitation of cells on sections

Ovaries, fixed or non-fixed depending on activity of the antibodies to be used, were used for 3 μm cryosections. Prior to staining, all sections were blocked in 3% BSA with mAb to CD16/32. For multi-color staining, antibodies which were directly conjugated to a fluorescent dye were used. If biotin labeled antibodies were used, this antibody was used for the first staining after blocking with a biotin and avidin blocking kit from Vector BioLab (Philadelphia, PA, USA). Fluorescent dye-labeled streptavidin was then used as secondary reagent. Due to general high autofluorescence background in ovaries, we used APC labeled antibodies for staining ST2 and mTOR, because the APC emission peak is close to near infrared where ovaries do not emit autofluorescence. We designated purple color for APC. In each case, staining included an Ig isotype control. The sections were observed by a fluorescent microscope (Nikon Eclipse Ni, Tokyo, Japan) or a confocal microscope (Nikon Eclipse Ti), and digital images were captured and analyzed with NIS Elements 3.2 from Nikon. For quantitation of $ST2^+$ cells, consecutive images were captured with a Nikon Instruments Eclipse 80i with motorized stage, and combined to a single image of the entire section at x200. On captured images, each follicle was outlined and total granulosa cells and those of $ST2^+$ were counted and calculated as % of $ST2^+$ cells (i.e., $ST2^+$ granulosa/total granulosa x100). $ST2^+$ cells in interstitial tissue with area 50 × 50 μm^2 were also counted.

Classification of early atretic follicles

We have previously shown that autophagy and macrophage invasion occur at early stages of atresia. Classification of early atretic follicles was established by using a combination of two markers, i.e., TUNEL in oocytes/granulosa, and IA/IE^+ macrophage invasion of follicles: (1) *normal*, $TUNEL^-IA/IE^-$; (2) *early stage*, $TUNEL^+IA/IE^-$; and (3) *early-middle stage*, $TUNEL^-IA/IE^+$ [8, 16]. Immunofluorescent TUNEL was performed with a kit (In Situ Cell Death Detection Kit, Fluorescein Roche, Nutley, NJ, USA), and was co-stained with other markers. For the best morphology of atretic follicles, TUNEL was also performed by immunohistochemistry (IHC) on one of serial sections to match with other immunofluorescent markers. Immunofluorescence on zona pellucida (ZP) was sometime used as an additional marker.

Detection of genome wide gene expression in ovaries post eCG/hCG treatment

After treatment with eCG/hCG, ovaries from three mice were harvested at each time point (i.e., 0, 6, 9, 13 h). One was immediately used for isolation of total ovarian RNA, and 300 ng were used for amplification and purification with Illumina TotalPrep RNA Amplification Kit (Illumina, San Diego, CA, USA) following kit instructions. After quality testing, the samples were submitted to the DNA Microarray Core facility at The University of Texas Health Science Center at Houston for detection of genome wide gene expression patterns following a published method [16] utilizing Illumina Sentrix Beadchip Array Mouse Ref8_v2 arrays. After hybridization, the arrays were scanned with BeadArray Reader (Illumina). Data were first analyzed with GenomeStudio software (Illumina) for reliability and consistence. Analysis showed that three samples at each time point clustered closely together, demonstrating the reliability of the data. Expression levels for each gene were calculated into geometry means of fluorescent signal intensity with a standard software.

Conventional or quantitative RT-PCR detection of mRNA

Complementary DNA was synthesized using 1 μg of total RNA through an reverse transcription (RT) reaction (RNA PCR Core Kit, Applied Biosystems, Foster City, CA, USA). Conventional polymerase chain reaction (PCR) was carried out to detect mRNA (Table 1). The products were separated by electrophoresis in 1.5% agarose gel, stained with ethidium bromide, and visualized under UV light illumination. Digital images were captured by an imaging analyzer (PerkinElmer, Waltham, MA, USA). Quantitative PCR (Q-PCR) was performed with a pair of primers for various genes under similar conditions as for conventional PCR using the SYBR Green system (SuperArray Bioscience, Frederick, MD, USA) on iCycler-iQ thermocycler (BioRad, Hercules, CA, USA). Relative abundance was calculated as $2^{\Delta(t\text{-}t_0)}$ following a published method [29]. A mouse house-keeper gene *Gapdh* was used as a control.

Statistics

Unpaired *t*-test was used for data comparison between two groups. One-way ANOVA with Dunnett's post-HOC test

Table 1. Primers, product DNA lengths, and annealing temperature for PCR on selected genes in ovaries

Gene	Forward	Reversed	*bp*	t_{anneal}
St2l	GATGTCCTGTGGCAGATTAACA	AGCAACCTCAATCCAGAACACT	333	56
St2s	GGCTCTCACTTCTTGGCTGA	ACAACCAAGTAAGGAGTGTCC	260	57
1133	GCTGCGTCTGTTGACACATT	GACTTGCAGGACAGGGAGAC	222	58
mTor	TGTGCCAGGAACATACGACC	TTGCTGCCCATCAGAGTCAG	117	57
Il6	GAGGATACCACTCCCAACAGACC	AAGTGCATCATCGTTGTTCATACA	141	58
Il1b	TGGCTGTGGAGAAGCTGTGGC	TGAGTCACAGAGGATGGGCTC	116	60
Ccl6	CACCAGTGGTGGGTGCATCAAG	GTGCTTAGGCACCTCTGAACTC	106	58
Ccl9	CCCTCTCCTTCCTCATTCTTACA	AGTCTTGAAAGCCCATGTGAAA	141	55
Gapdh	ACTCCACTCACGGCAAATTC	TCTCCATGGTGGTGAAGACA	157	58

for comparison among more than two groups (GraphPad Prism7). $P < 0.05$ is considered as significant. Each group on graphs was expressed as mean ± SD.

Results

Transient expression of IL33 receptor ST2 in granulosa of early atretic follicles

The expression pattern of *St2 (Il1rl1)* and co-receptor *Il1rap* was examined post-hCG injection at the mRNA level. DNA microarray data showed that *St2* mRNA in the ovaries was elevated after hCG injection and peaked at 6 h (Figure 1A), which was slightly delayed for approximately 3 h from the expression peak for *Il33* (Figure 1B). *St2* expression gradually dropped but was sustained at relatively high levels thereafter. On the other hand, co-receptor *Il1rap* was relatively stable during the hCG treatment period (Figure 1A). The RT-PCR demonstrated a similar tendency (Figure 1B). *St2* is expressed in two isoforms, i.e., membrane-bound *St2l* and soluble *St2s* due to different splicing. While ST2l serves as an IL33 receptor, ST2S is a decoy. The RT-PCR did not detect any S*t2s* in ovaries. As a technical control to verify RT-PCR on *St2s*, expression of *St2s* in a kidney sample, which is known to express *St2s*, was detectable (Figure 1B). It was concluded that ovaries expressed *St2l* that is a membrane-bound IL33 receptor, but not *St2s* that is negative regulation of IL33 as a decoy.

Next, immunofluorescence was performed for ST2 expression at the protein level. ST2 was detected in granulosa cells of early stage of atretic follicles that were TUNEL$^+$ in oocyte and granulosa (Figure 2A). Morphological observations on these follicles with ST2 expression on granulosa also showed signs of atresia that include abnormal ZP shrinkage and condensed nuclei in some granulosa cells (Figure 2A). ST2 was not observed in the early-middle stage of atretic follicles, i.e., with IA/IE$^+$ macrophages (Figure 2B). ST2 was not detected in normal follicles nor other tissue locations (Figure 2A and B). Statistical analysis confirmed that ST2 was significantly expressed in granulosa of early stage atretic follicles, i.e., with apoptotic oocyte and granulosa ($***P < 0.001$) (Figure 2C).

Activation of NFκB pathway in granulosa of atretic follicles

To further determine whether ST2 on granulosa of atretic follicles triggered the NFκB transcription pathway in early atretic follicles, $Tg^{(NFkB\text{-}RE\text{-}Luc)}$ mice, in which activation of the NFκB pathway can be detected by transgenic luciferase reporter mediated bioluminescence, were utilized. First, whole body scanning of mice after injection of D-luciferin revealed bioluminescence of various intensities in both ovarian areas (designated as *ROI*1 and *ROI*2, and indicated by white arrows in Figure 3A) in randomly selected five females of 8–10 weeks of age. By contrast, there was no bioluminescence in the same area in any of four age-matched males (Figure 3A and B). On the other hand, similar bioluminescent patterns/density were observed in both genders in neutral region, e.g., thymic area (*ROI*3, indicated by red arrows in Figure 3A). Thus, detected bioluminescence in females was most likely emitted from ovaries. Since ST2 expression peaked after 6 h post-hCG injection, three Tg mice at 9 h after hCG injection were examined. Their ovaries showed significantly higher bioluminescent densities than those of randomly selected mice (Figure 3B).

Next, it was examined whether this NFκB activation was occurring in atretic follicles. For this, a unique method was developed for microscopic localization of bioluminescence using non-fixed thick frozen (10 μm) sections to preserve luciferase activity. On three ovaries of $Tg^{(NFkB\text{-}RE\text{-}Luc)}$ mice at 9 h post-hCG injection, bioluminescence was localized to granulosa cells of follicles at early stage of atresia with TUNEL$^+$ oocyte/granulosa (Figure 3C); a total nine atretic follicles in those ovaries were observed. Bioluminescence was not detected in any normal follicles ($n = 9$) (Figure 3C). To further confirm the above results, immunofluorescence was performed to localize luciferase protein in combination with other markers, i.e., ZP and TUNEL (Figure 3D). It was again shown that luciferase activity was located in the cytoplasm of granulosa cells of early atretic follicles with TUNEL$^+$ granulosa/oocyte (Figure 3D), in agreement of bioluminescent detection of NFκB activity (Figure 3C). Luciferase was not detected in normal follicles (Figure 3D). It was therefore concluded that NFκB activation is occurring in granulosa cells at early stage of atresia.

Expression of inflammatory and autophagy associated molecules in ovaries post-hCG injection

Next, it was investigated what were potential target genes for activated NFκB transcription pathway in atretic follicles post-hCG injection. Two categories of molecules were focused on that were associated with: (1) macrophage trafficking or migration, i.e., inflammatory molecules including cytokines, chemokines, and adhesion molecules; and (2) autophagosome and autophagy regulation. Through analyses on global gene expression DNA microarray data from ovaries 0, 6, 9, 13 h post-hCG injection ($n = 3$ per time point), those genes can be classified into four expression patterns: (1) expression fluctuated together with IL33 expression, (2) expression

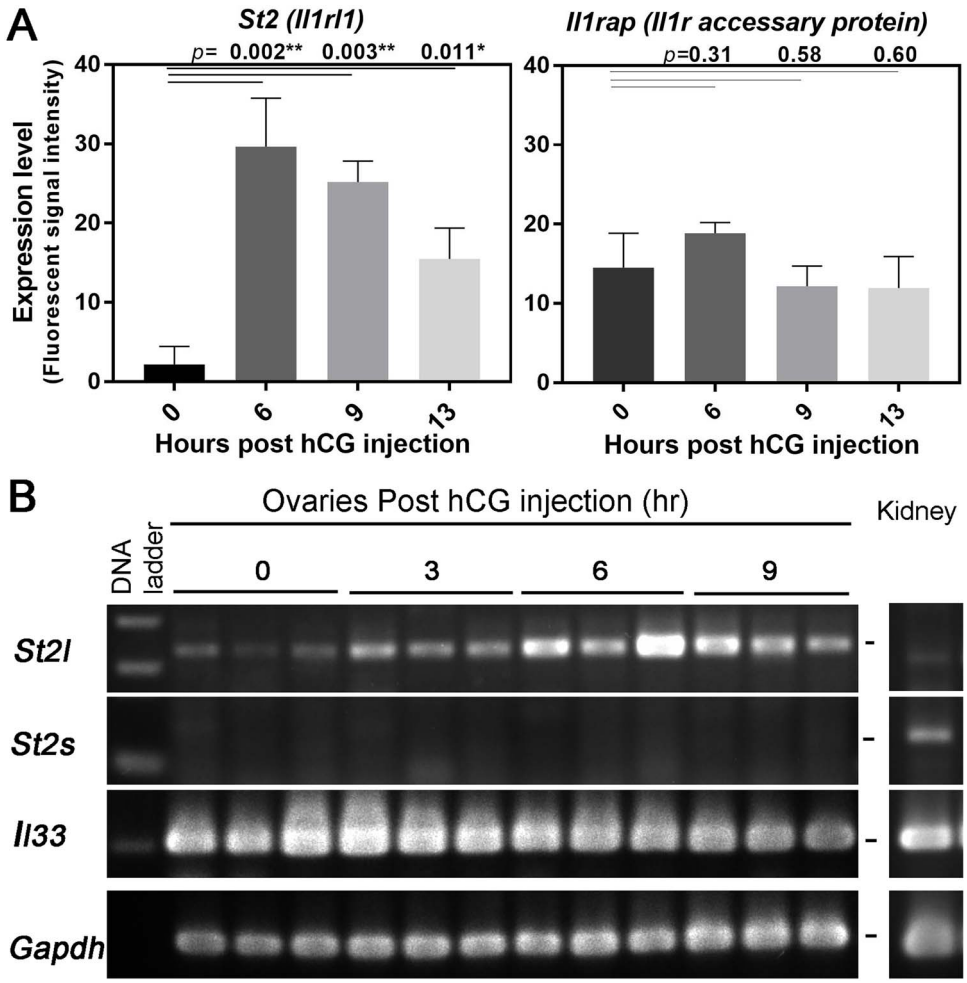

Figure 1. Expression of *Il33* and its receptor *St2* post eCG/hCG treatment. (A) DNA Microarray assay shows up-regulation of *St2* (*Il1rl1*) expression post-hCG injection, while expression of co-receptor *Il1rap* (*IL1R accessary protein*) remains unchanged; $n=3$, gene expression levels are shown as fluorescent signal intensity; *P*-values for each time point compared to 0 h (one-way ANOVA with Dunnett's post-HOC test) are indicated. (B) RT-PCR on ovarian *Il33* and *St2* expression post-hCG injection reveals upregulation of *St2l* (membrane-bound form); note that *St2s* (soluble form) is not detectable in ovaries; a kidney tissue serves as positive control for PCR as it expresses both *St2l* and *St2s*. Three of six samples/time point are shown.

delayed from IL33 expression, (3) stable expression without significant changes, and (4) expression reduced. The results are summarized in Figure 4. *Pattern 1* includes inflammatory cytokines *Il1b*, *Il11*, and *Bcl3* (a NFκB regulator/modulator), which peaked at 6 h post-hCG injection (Figure 4A). *Pattern 2* includes inflammatory cytokine *Il6*, chemokines *Ccl6* and *Ccl9*, and adhesion molecule *Icam1*, whose expression gradually plateaued around 9 h (red lines in Figure 4A and B). *Pattern 3* includes many inflammatory molecules and those involved in autophagosome formation, such as *Lc3* and *Atg*s, whose expression was stable (Figure 4A–C). *Pattern 4* had only one gene, *mTor*. Its expression rapidly reduced after 6 h to a low level (red line in Figure 4C). Obviously, stable expression of genes in *Pattern 3* imply that they are not likely to be the targets of the NFκB pathway.

Antibody blockage of IL33 or Il33 KO reduces NFκB activation and alters expression of IL6 and mTOR in ovaries

It was then investigated whether antibody blockage of IL33 or Il33 KO could inhibit activation of NFκB. If so, it could be assumed that a gene whose expression was inhibited or altered by IL33 blockage or IL33 gene deletion (KO) could be a target for the NFκB transcription pathway. It has been previously shown that IL33 antibody or IL33 KO has no effect on ovulation [8, 16]. A recent paper reported inactivation of NFκB in ovulating follicles [28]. Thus, blockage of NFκB would not affect ovulation-related genes. Three $Tg^{(NFkB\text{-}RE\text{-}Luc)}$ female mice were injected with anti-IL33 neutralization antibody while another three injected with rat IgG isotype before eCG/hCG injection. Bioluminescent intensities in ovarian areas (*ROI1*/*ROI2*) were scanned at 9 h post-hCG injection. Statistical analysis showed a significant reduction of NFκB activity in ovaries ($n=2\times3$, $*P=0.049$, Figure 3B). In another set of experiments using *WT* B6 mice with a similar protocol, it was examined whether ST2 expression was affected by the antibody blockage or in IL33 KO, i.e., $Il33^{-/-}$ mice (five mice/group). Immunofluorescence showed that IL33 antibody blockage did not alter expression of ST2 in granulosa cells of early atretic follicles, and $Il33^{-/-}$ mice showed an identical ST2 expression pattern (Figure 5A and B), suggesting that ST2 expression was independent of IL33-NFκB regulation. In fact, ST2 expression in $Il33^{-/-}$ mice appeared more persistent and profound than those *WT* group. Expression of potential NFκB target genes

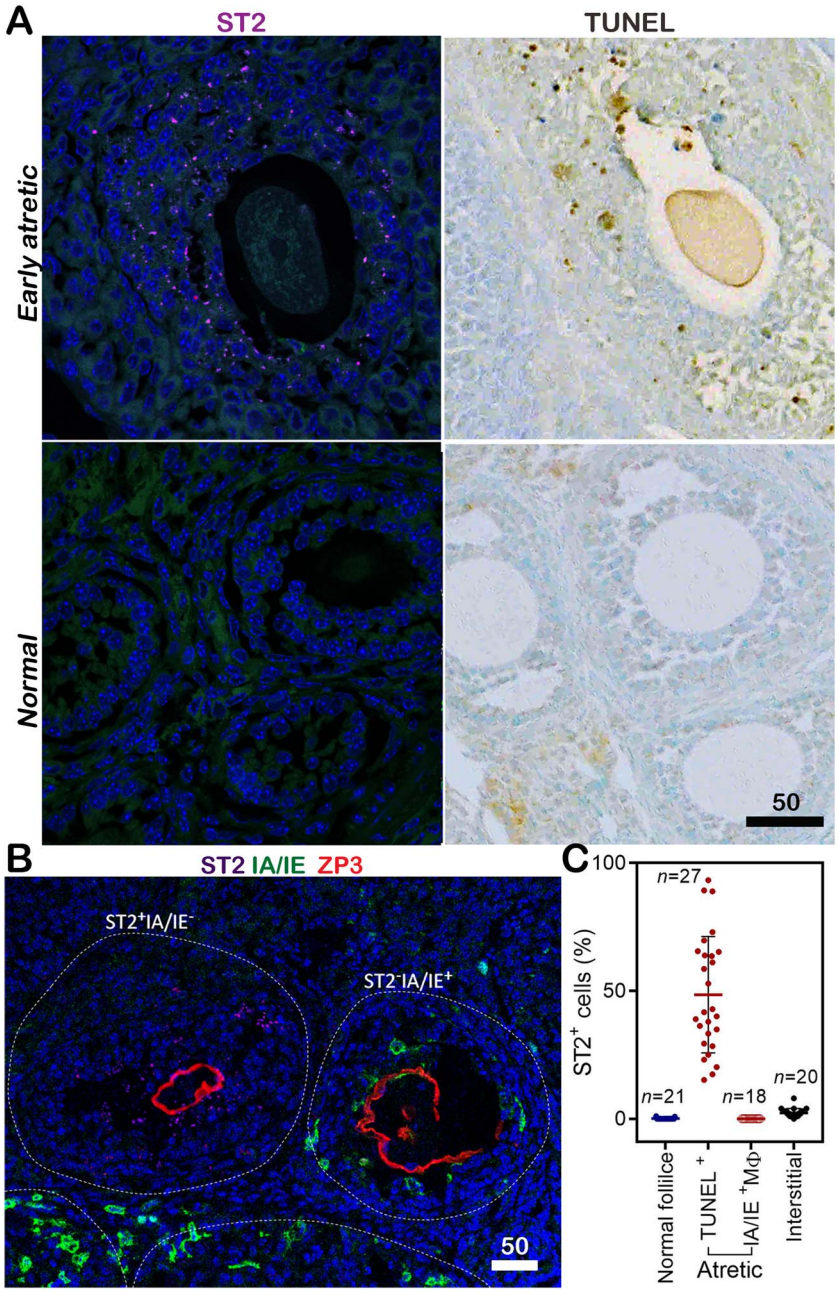

Figure 2. ST2 expression in granulosa cells of early atretic follicles before macrophage invasion. (A) Immunofluorescence shows ST2 (purple) in an atretic follicle at early stage, as demonstrated by apoptotic oocyte and granulosa cells on TUNEL staining on an adjacent serial section; ST2 was absent in normal developing follicles. Nuclei were counter stained by DAPI (blue). (B) Immunofluorescence shows ST2 expression in an atretic follicle without IA/IE$^+$ macrophages (labeled as ST2$^+$IA/IE$^-$), but not in the adjacent ones with invasion of IA/IE$^+$ macrophages (green)(labeled as ST2$^-$IA/IE$^+$); follicles are outlined by white dotted lines; ZP was counter-stained as red. (C) One-way ANOVA analysis shows significantly higher ST2 expression in early atretic follicles of TUNEL$^+$ than those with IA/IE$^+$ macrophages (MΦ); each dot represents % of ST2$^+$ granulosa in one follicle. Follicles on sections from six ovaries were countered for ST2$^+$ cells. Bar units, μm.

in ovaries was investigated. These genes include Il6, Icam1, Ccl6, Ccl9, and mTOR (red lines in Figure 4), because they were not only related to macrophage invasion and autophagy, but also slightly delayed from IL33 surge. Both conventional RT-PCR and Q-PCR were performed using ovarian RNA. *Il33*$^{-/-}$ ovaries showed >10 folds lower *Il6* expression than *WT* (Figure 6A and B), while their *Il1b* expression was comparable. By contrast, *Il33*$^{-/-}$ ovaries showed elevated *mTor* expression from 2 to >16-fold as compared to *WT* (Figure 6A and B). Increased mTOR expression in the granulosa cells in *Il33*$^{-/-}$ ovaries was also demonstratable at the protein level by immunofluorescence (Figure 5C). Mean fluorescent intensity of mTOR was assessed in early atretic follicles (i.e., TUNEL$^+$) among three groups (10 follicles from 3 individuals/group). Statistical analysis showed significantly higher mTOR intensity in *Il33*$^{-/-}$ mice than *WT* mice (Figure 5D). IL33 blockage also showed similar but less prominent results (Figures 5 and 6). In summary, as compared to *WT* mice, *Il33*$^{-/-}$ ovaries or those after IL33 blockage showed significantly reduced IL6 expression, but

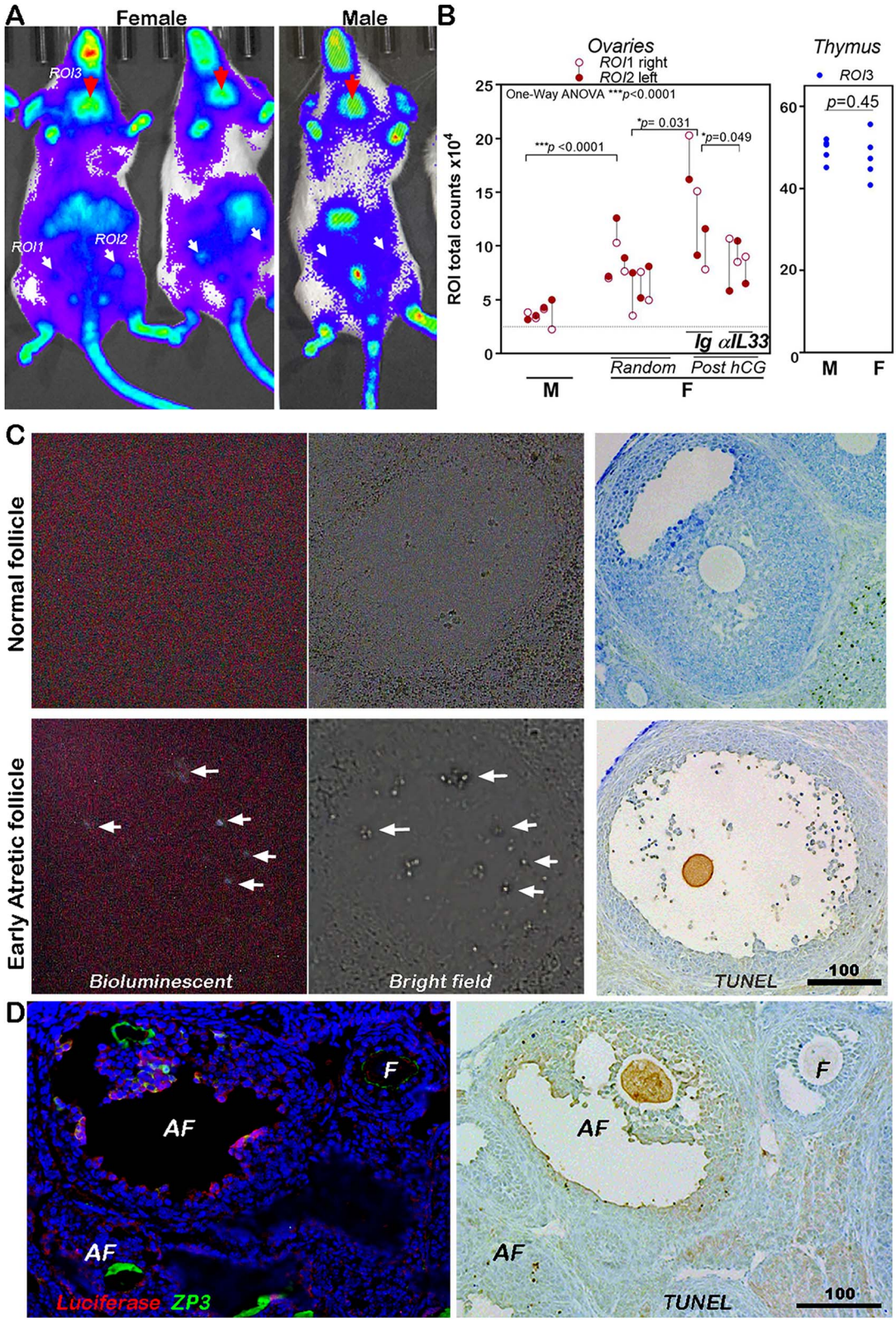

Figure 3. Activation of NFκB transcription pathway in granulosa of early atretic follicles as revealed by bioluminescence in mice with transgenic NFκB activating element-luciferase reporter. (A) Whole-body scanning after injection with D-luciferin shows luminescence in ovaries (*ROI*1 and 2, white arrows) in females, but not in similar areas of a male; note similar luminescent intensity in thymus (red arrows, *ROI*3) in both genders. *ROI*, Region of Interest. (B) Statistical summary of luminescent intensities for paired ovaries (*ROI*1 and *ROI*2) and thymus (*ROI*3). Note that hCG injection increased ovarian luminescent intensities, while IL33 antibody (*α-IL33*) inhibited the increase; females and males show similar intensities in thymus. *Ig*, IgG isotype control. (C) Microscopic location of luminescence on frozen section reveals activation of NFκB in granulosa cells (arrows) in a TUNEL$^+$ early atretic follicle, but absent in a normal follicle. (D) Immunofluorescence shows luciferase (red) in granulosa of TUNEL$^+$ early atretic follicles (AF), but not in an adjacent normal one (F). ZP was counter stained as green. Three ovaries from hCG injected Tg mice were observed. Bar units, μm.

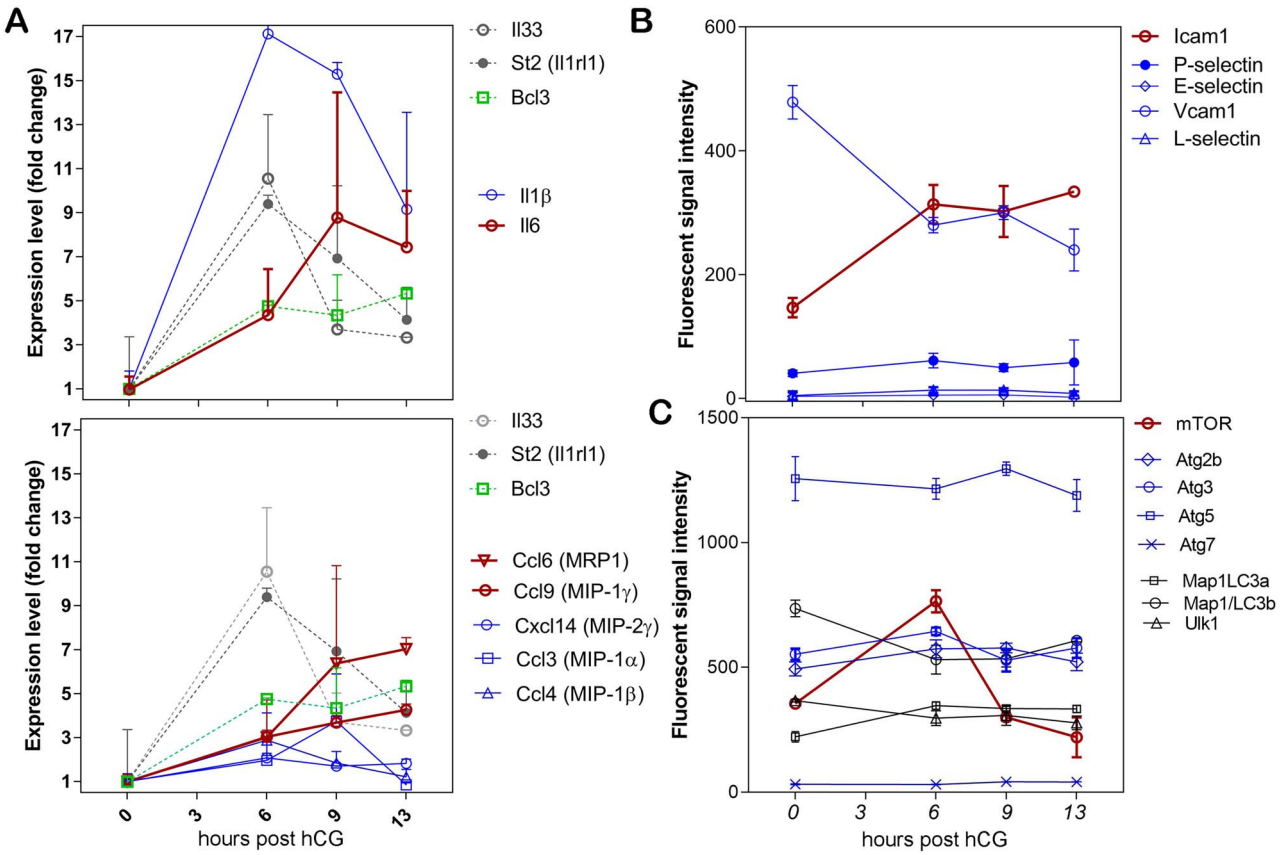

Figure 4. Ovarian expression of inflammatory and autophagy-associated molecules post-hCG injection as detected by DNA microarray. Fluorescent signal density for each gene at 0 h was defined as baseline, and expression levels for other time points are shown as fold changes relative to this baseline. (A) Expression of cytokines and chemokines. *Il33*, *St2*, and *Bcl3* (NFκB modulator) are included in each panel for comparison. (B) Expression of adhesion molecules; (C) Expression of genes associated with autophagy. Those labeled with red line and symbols are potentially regulated by activation of IL33–ST2–NFκB axis.

higher mTOR expression. These data suggest that IL6 and mTOR expression are likely associated with activation of the NFκB pathway. Although reduction in *Ccl6* and *Ccl9* expression in IL33 blockage or *IL33*$^{-/-}$ mice was observed, it was not statistically significant (Figure 6B), suggesting their complicated involvement in other ovarian physiological events [30].

Discussion

It has been previously shown that IL33 is required for autophagy in granulosa cells and macrophage invasion of atretic follicles in order to seamlessly dispose of atretic follicles with minimal remnants [8]. On the other hand, IL33 is not required for apoptosis during atresia. It has been shown that apoptosis alone is not sufficient for full disposal of atretic follicles, as IL33 deficiency causes accumulation of massive collapsing atretic follicles, which emit harmful oxidative substances and lipofuscins. As a result, IL33 deficient mice show shrunken oocyte reservoirs and shortened reproductive lifespan. In this study, it was further revealed that IL33's involvement in atresia is through activation of the NFκB pathway in granulosa cells at an early stage of atresia. Activation of NFκB pathway in ovaries *in vivo* was first observed, and the activation was further localized to granulosa cells in early atretic follicles in Tg mice with luciferase-reporter for NFκB activation. Since this study involved eCG/hCG injection, it was necessary to ask if activated NFκB is involved in ovulation. A recent study has shown inactivation of NFκB pathway in ovulating follicles by progesterone receptor is necessary for successful ovulation [28]. Furthermore, a previous study has shown that IL33 deficiency or blockage does not affect ovulation [8, 16]. Thus, the detected NFκB activity in ovaries could therefore be assumed to be more related to atresia than ovulation. The results for NFκB activation in early atretic follicles were also supported by the observation of a transient expression of IL33 receptor ST2 in granulosa cells at early atresia at both the RNA and protein level. Antibody blockage of IL33 or IL33 deficiency reduced ovarian NFκB activation, but had no effect on ST2 expression. It suggests that expression of ST2 is independent of IL33. Taken together, it is concluded that IL33 activates the ST2–NFκB axis in the granulosa cells of early atretic follicles, though it has yet to be determined which pathway, the canonical or alternative one, is activated [31]. This conclusion is also supported by several previous studies. Activation of NFκB in ovaries has been reported [32]. Interestingly, multiple studies have linked inactivation of the NFκB pathway to ovarian disease, e.g., premature ovarian failure or poly cystic ovarian syndrome [33, 34]. It will be of interest to ask if inactivation of NFκB in ovaries may be related to accumulation of collapsing follicles as seen in our *Il33*$^{-/-}$ mice.

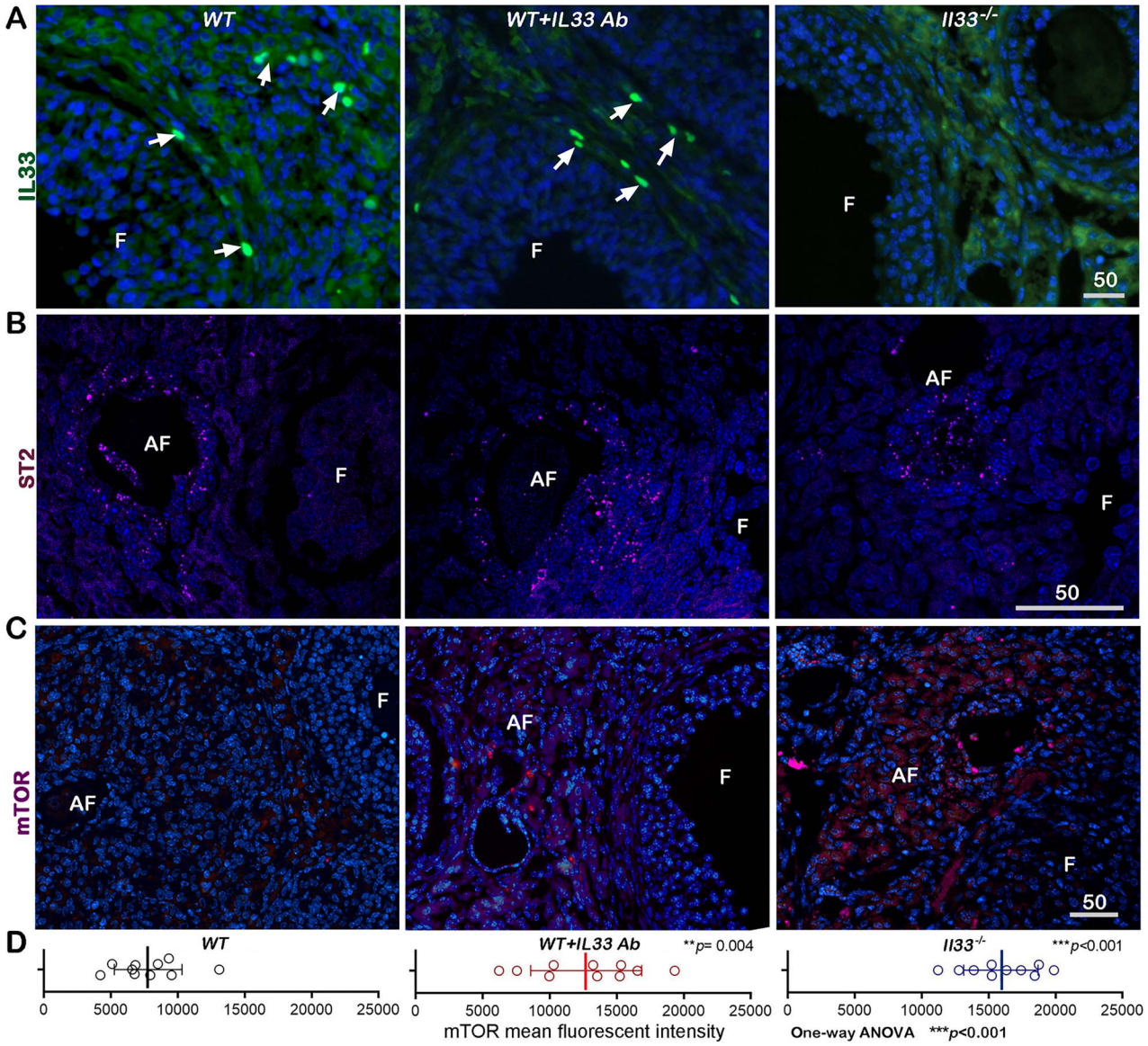

Figure 5. Antibody IL33 blockage or IL33 KO (*Il33*$^{-/-}$) does not affect ST2 expression but significantly increases mTOR expression in granulosa cells in early atretic follicles. For IL33 blockage, neutralizing IL33 antibody (*WT*+ *IL33 Ab*) or rat IgG (*WT*) was injected before eCG/hCG treatment, and ovaries were sampled at 9 h post-hCG injection. (A) Immunofluorescence shows nuclear IL33 (green, arrow) of thecal cells in *WT* and *WT*+ *IL33 Ab* group, while IL33 was absent in *Il33*$^{-/-}$ ovaries. (B) Immunofluorescence reveals ST2 (purple) expression in granulosa cells of early atretic follicle (AF) in all three groups; note absence of ST2 in adjacent normal follicles (*F*). (C) mTOR (purple) is nearly undetectable in atretic follicles (*AF*) in *WT* ovaries. By contrast, elevated or clustered mTOR proteins are present in atretic follicles in both *WT*+ *IL33 Ab* and *Il33*$^{-/-}$ mice. (D) Statistical summary of mTOR protein level in TUNEL^{+} early atretic follicles; 10 follicles from 3 ovaries from each group were analyzed by one-way ANOVA with Dunnett's post-HOC test; *P*-values with comparison to *WT* group are shown. mTOR level in each TUNEL^{+} atretic follicle was measured as mean fluorescent intensity for mTOR staining on 2-color immunofluorescent images for mTOR (purple) and TUNEL (green) by Nikon Element, and shown as a dot. Bar units, μm.

The current study did not intend to identify all genes that were targets of the NFκB transcription pathway in granulosa during atresia. However, microarray data on global gene expression and RT-PCR suggests the likely roles of the IL33-NFκB axis in regulation of autophagy and macrophage recruitment during atresia. First, it was differentially identified IL6 and mTOR whose expression were either up- or down-regulated after antibody blockage or in *Il33*$^{-/-}$ mice. Thus, expression of those two genes is potentially controlled by IL33–ST2–NFκB axis. Second, many previous studies have revealed a potential role of macrophage invasion and autophagy in granulosa in disposal of atretic follicles. IL6, a proinflammatory cytokine, is a known main target gene for the NFκB pathway [35]. Expression of IL6 by follicular cells has been also reported [36]. IL6's role in proinflammatory responses including macrophage recruitment is well known. Third, this study also suggests the involvement of IL33-NFκB axis in upregulation of autophagy in granulosa. As discussed earlier, autophagic activity is largely regulated by other cellular pathways. Results from this study indeed show that expression of autophagosome-associated genes (i.e., atg7, atg9, atg5, and LC3) did not change by IL33 blockage or in *Il33*$^{-/-}$ ovaries. However, mTOR, a critical negative regulator of autophagy, significantly increased in both *Il33*$^{-/-}$ ovaries

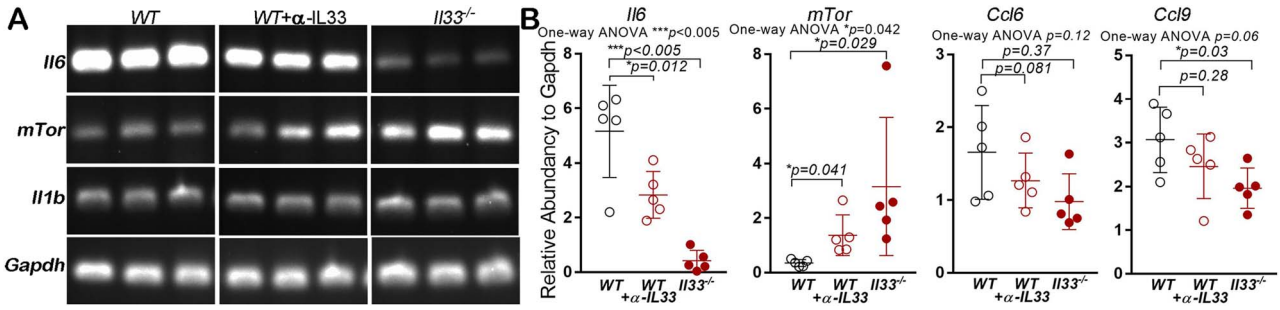

Figure 6. IL33 KO (*Il33*$^{-/-}$) or antibody IL33 blockage alters ovarian expression of IL6 and mTOR. For blockage of IL33, neutralizing antibody (*WT* + *IL33 Ab*) or rat IgG (*WT*) was injected before eCG/hCG treatment, and ovaries were sampled at 9 h post-hCG injection. (A) Conventional RT-PCR shows downregulation of *Il6* and upregulation of *mTor* in both *Il33*$^{-/-}$ and *WT* + *IL33 Ab* mice; note unchanged *Il1b* expression. Three of five samples/group are shown. (B) Summary for Q-PCR on selected ovarian gene expression. Total RNA was isolated from ovaries 9 h post-hCG injection; results are expressed as relative abundancy as compared to *Gapdh* of the same sample [29]. $n = 5$.

and after IL33 blockage, resulting in diminished autophagy in granulosa cells [8]. One may question how inhibition of IL33-NFκB axis would greatly upregulate mTOR expression, as mTOR is not a known target for NFκB. Yet NFκB's regulation of autophagy has been well documented, especially in disposal of large quantities of tissues [22–24]. One way for NFκB pathway to boost autophagy is to up-regulate expression of miRNA (e.g., miR100 and miR101), which inhibits mTOR expression at the transcriptional or translational level [25, 37, 38]. Autophagy activity is regulated by cellular signaling or modification of pathways, such as mTOR [26, 27]. Results from this study suggest that it may also be the case for atresia. Currently, it is being investigated whether miRNA is involved in down-regulation of mTOR in our model. Finally, it is worthwhile to mention several studies that link defects in autophagy to ovarian disease. mTOR has been implicated in premature ovarian insufficiency (POI) [39]. Variant Atg7 and Atg9 are associated human POI probably due to insufficient lysosome degradation pathway activity [40]. Failure of autophagy in granulosa has been linked to POI [41].

In summary, serial studies have revealed more detailed mechanisms for atresia beyond apoptosis. It was previously shown that apoptosis is not sufficient to fully dispose of all dead cells from atretic follicles without any harmful wastes. IL33-mediated disposal of those dead cells is one essential step of atresia for keeping a healthy ovarian environment allowing for normal function. This discovery may provide a novel hypothesis for idiopathic POI. Mounting evidence suggests the role of ROS and oxidative stress (OS) in idiopathic POI [42–47]. For example, mutation in mitochondria may cause elevation of ROS/OS in ovaries [48]. Abnormal aging in ovaries increase ROSs levels [49, 50]. This study suggests that incomplete disposal of atretic follicles may be another potential factor for increased ROS during ovarian aging. It was shown previously that undisposed atretic follicles collapse and degrade in *IL33*$^{-/-}$ ovaries, leading to accumulation of harmful substances, such as lipofuscin and ROSs [8]. Recently, it was demonstrated that those harmful substances in *Il33*$^{-/-}$ ovaries leak to near-by developing follicles and causes OS there (Lou et al., unpublished data). Consequently, the *IL33*$^{-/-}$ females show shrunken oocyte reservoirs and significantly shortened reproductive lifespan, which are the characteristics of human POI. One of our long-term goals is to determine if deficiency in disposal of atretic follicles is one cause for POI in humans.

Acknowledgment

Global gene expression detection using DNA microarray was performed at Quantitative Genomics & Microarray Service Center, The University of Texas HSC at Houston. Drs. G. Trible and C. Carlock edited the manuscript.

Conflict of Interest

The authors have declared that no conflict of interest exists.

Authors' contributions

JW performed experiments and analyzed data. CC designed and performed experiments, and analyzed data. KT performed experiments. JS performed experiments and analyzed data. CZ designed and performed experiments. YL conceived the study and wrote paper.

Data availability

The data underlying this article will be shared on reasonable request to the corresponding author.

References

1. Tilly JL, Kowalski KI, Johnson AL, Hsueh AJ. Involvement of apoptosis in ovarian follicular atresia and postovulatory regression. *Endocrinology* 1991; **129**:2799–2801.
2. Lee CY, Baehrecke EH. Steroid regulation of autophagic programmed cell death during development. *Development* 2001; **128**: 1443–1455.
3. Thomé RG, Santos HB, Arantes FP, Domingos FTT, Bazzoli N, Rizzo E. Dual roles for autophagy during follicular atresia in fish ovary. *Autophagy* 2009; **5**:117–119.
4. Choi J, Jo MW, Lee EY, Yoon BK, Choi DS. The role of autophagy in follicular development and atresia in rat granulosa cells. *Fertil Steril* 2010; **93**:2532–2537.
5. Hułas-Stasiak M, Gawron A. Follicular atresia in the prepubertal spiny mouse (*Acomys cahirinus*) ovary. *Apoptosis* 2011; **16**: 967–975.
6. Escobar ML, Echeverra OM, Vazquez-Nin GH. Immunohistochemical and ultrastructural visualization of different routes of oocyte elimination in adult rats. *Eur J Histochem* 2012; **56**:17.
7. Escobar ML, Echeverría OM, García G, Ortíz R, Vázquez-Nin GH. Immunohistochemical and ultrastructural study of the lamellae of oocytes in atretic follicles in relation to different processes of cell death. *Eur J Histochem* 2015; **59**:2535.

8. Wu J, Carlock C, Zhou C, Nakae S, Hicks J, Adams HP, Lou Y. IL-33 is required for disposal of unnecessary cells during ovarian atresia through regulation of autophagy and macrophage migration. *J Immunol* 2015; **194**:2140–2147.
9. Tanida I, Ueno T, Kominami E. LC3 and autophagy. *Methods Mol Biol* 2008; **445**:77–88.
10. Gudmundsson S, Kahlhofer J, Baylac N, Kallio K, Eskelinen EL. Correlative light and electron microscopy of autophagosomes. *Methods Mol Biol* 2019; **1880**:199–209.
11. Meng L, Jan SZ, Hamer G, van Pelt AM, van der Stelt KJ, Teerds K. Preantral follicular atresia occurs mainly through autophagy, while antral follicles degenerate mostly through apoptosis. *Biol Reprod* 2018; **99**:853–863.
12. Carlock C, Wu J, Zhou C, Ross A, Adams H, Lou Y. Ovarian phagocyte subsets and their distinct tissue distribution patterns. *Reproduction* 2013; **146**:491–500.
13. Oboki K, Ohno T, Kajiwara N, Arae K, Morita H, Ishii A, Nambu A, Abe T, Kiyonari H, Matsumoto K, Sudo K, Okumura K, *et al*. IL-33 is a crucial amplifier of innate rather than acquired immunity. *Proc Natl Acad Sci U S A* 2010; **107**:18581–18586.
14. Lefrancais E, Roga S, Gautier V, Gonzalez-de-Peredo A, Monsarrat B, Girard J-P, Cayrol C. IL-33 is processed into mature bioactive forms by neutrophil elastase and cathepsin G. *Proc Natl Acad Sci U S A* 2012; **109**:1673–1678.
15. Kakkar R, Lee R. The IL-33/ST2 pathway: therapeutic target and novel biomarker. *Nat Rev Drug Discov* 2008; **7**: 827–840.
16. Carlock C, Wu J, Zhou C, Tatum K, Adams HP, Tan F, Lou Y. Unique temporal and spatial expression patterns of IL-33 in ovaries during ovulation and estrous cycle are associated with ovarian tissue homeostasis. *J Immunol* 2014; **193**: 161–169.
17. Carlock C, Wu J, Shim J, Moreno-Gonzalez I, Pitcher M, Quevedo J, Hicks J, Suzuki A, Iwata J, Lou Y. Interleukin33 deficiency causes tau abnormality and neurodegeneration with Alzheimer-like symptoms in aged mice. *Transl Psychiatry* 2017; **7**: e1164.
18. Wu J, Shim J, Carlock C, Moreno-Gonzalez I, Glass W II, Ross A, Barichello T, Quevedo J, Lou Y. Requirement of brain interleukin33 for aquaporin4 expression in astrocytes and glymphatic drainage of abnormal tau. *Mol Psychiatry* 2021; **26**: 5912–5924.
19. Klionsky DJ, Abeliovich H, Agostinis P, Agrawal DK, Aliev G, Askew DS, Baba M, Baehrecke EH, Bahr BA, Ballabio A, Bamber BA, Bassham DC, *et al*. Guidelines for the use and interpretation of assays for monitoring autophagy in higher eukaryotes. *Autophagy* 2012; **8**:445–544.
20. Barth S, Glick D, Macleod KF. Autophagy: assays and artifacts. *J Pathol* 2010; **221**:117–124.
21. Mizushima N, Yoshimori T, Levine B. Methods in mammalian autophagy research. *Cell* 2010; **140**:313–326.
22. Trocoli A, Djavaheri-Mergny M. The complex interplay between autophagy and NF-κB signaling pathways in cancer cells. *Am J Cancer Res* 2011; **1**:629–649.
23. Su Z, Yang Z, Xu Y, Chen Y, Yu Q. Apoptosis, autophagy, necroptosis, and cancer metastasis. *Mol Cancer* 2015; **14**: 48.
24. Verzella D, Pescatore A, Capece D, Vecchiotti D, Ursini MV, Franzoso G, Alesse E, Zazzeroni F. Life, death, and autophagy in cancer: NF-κB turns up everywhere. *Cell Death Dis* 2020; **11**: 210.
25. Liu X, Zhong L, Li P, Zhao P. MicroRNA-100 enhances autophagy and suppresses migration and invasion of renal cell carcinoma cells via disruption of NOX4-dependent mTOR pathway. *Clin Transl Sci* 2022; **15**:567–575.
26. Kim J, Kundu M, Viollet B, Guan K. AMPK and mTOR regulate autophagy through direct phosphorylation of Ulk1. *Nat Cell Biol* 2011; **13**:132–141.
27. Dossou AS, Basu A. The emerging roles of mTORC1 in macromanaging autophagy. *Cancers (Basel)* 2019; **11**:1422.
28. Park CJ, Lin PC, Zhou S, Barakat R, Bashir ST, Choi JM, Cacioppo JA, Oakley OR, Duffy DM, Lydon JP, Ko CJ. Progesterone receptor serves the ovary as a trigger of ovulation and a terminator of inflammation. *Cell Rep* 2020; **31**:107496.
29. Schmittgen TD, Livak KJ. Analyzing real-time PCR data by the comparative C(T) method. *Nat Protoc* 2008; **3**:1101–1108.
30. Zhou C, Borillo J, Wu J, Torres L, Lou Y. Ovarian expression of chemokines and their receptors. *J Reprod Immunol* 2004; **63**:1–9.
31. Liu T, Zhang L, Joo D, Sun S. NF-κB signaling in inflammation. *Signal Transduct Target Ther* 2017; **2**:17023.
32. Wright CJ, Cari EL, Sandoval J, Bales E, Sam PK, Zarate MA, Polotsky AJ, Kallen AN, Johnson J. Control of murine primordial follicle growth activation by IκB/NFκB signaling. *Reprod Sci* 2020; **27**:2063–2074.
33. Luo X, Xu J, Zhao R, Qin J, Wang X, Yan Y, Wang L, Wang G, Yang X. The role of inactivated NF-κB in premature ovarian failure. *Am J Pathol* 2021; **192**:468–483.
34. He Z, Wang Y, Zhuan L, Li Y, Tang ZO, Wu Z, Ma Y. MIF-mediated NF-κB signaling pathway regulates the pathogenesis of polycystic ovary syndrome in rats. *Cytokine* 2021; **146**: 155632.
35. Tak PP, Firestein GS. NF-κB: a key role in inflammatory diseases. *J Clin Invest* 2001; **107**:7–11.
36. Samir M, Glister C, Mattar D, Laird M, Knight PG. Follicular expression of pro-inflammatory cytokines tumour necrosis factor-α (TNFα), interleukin 6 (IL6) and their receptors in cattle: TNFα, IL6 and macrophages suppress thecal androgen production in vitro. *Reproduction* 2017; **154**:35–49.
37. Gozuacik D, Akkoc Y, Ozturk DG, Kocak M. Autophagy-regulating microRNAs and cancer. *Front Oncol* 2017; **7**:65.
38. Liu M, Han T, Shi S, Chen E. Long noncoding RNA HAGLROS regulates cell apoptosis and autophagy in lipopolysaccharides-induced WI-38 cells via modulating miR-100/NF-κB axis. *Biochem Biophys Res Commun* 2018; **500**:589–596.
39. Rehnitz J, Messmer B, Bender U, Nguyen XP, Germeyer A, Hinderhofer K, Strowitzki T, Capp E. Activation of AKT/mammalian target of rapamycin signaling in the peripheral blood of women with premature ovarian insufficiency and its correlation with *FMR1* expression. *Reprod Biol Endocrinol* 2022; **20**:44.
40. Delcour C, Amazit L, Patino LC, Magnin F, Fagart J, Delemer B, Young J, Laissue P, Binart N, Beau I. ATG7 and ATG9A loss-of-function variants trigger autophagy impairment and ovarian failure. *Genet Med* 2019; **21**:930–938.
41. Dou X, Jin X, Chen X, Zhou Q, Chen H, Wen M, Chen W. Bu-Shen-Ning-Xin decoction alleviates premature ovarian insufficiency (POI) by regulating autophagy of granule cells through activating PI3K/AKT/mTOR pathway. *Gynecol Endocrinol* 2022; **38**:754–764.
42. Behrman H, Kodaman PH, Gao S. Oxidative stress and the ovary. *J Soc Gynecol Investig* 2001; **8**:S40–S42.
43. Ruder ERH, Hartman TJ, Blumberg J, Goldman MB. Oxidative stress and antioxidants: exposure and impact on female fertility. *Hum Reprod Update* 2008; **14**:345–357.
44. Venkatesh S, Kumar M, Sharma A, Kriplani A, Ammini AC, Talwar P, Agarwal A, Dada R. Oxidative stress and ATPase6 mutation is associated with primary ovarian insufficiency. *Arch Gynecol Obstet* 2010; **282**:313–318.
45. Kumar M, Pathak D, Venkatesh S, Kriplani A, Ammini AC, Dada R. Chromosomal abnormalities and oxidative stress in women with premature ovarian failure (POF). *Indian J Med Res* 2012; **135**: 92–97.
46. Luderer U. Ovarian toxicity from reactive oxygen species. *Vitam Horm* 2014; **94**:99–127.
47. Tokmak A, Yıldırım G, Sarıkaya E, Çınar M, Boğdaycıoğlu N, Yılmaz FM, Yılmaz N. Increased oxidative stress markers may be

a promising indicator of risk for primary ovarian insufficiency: a cross-sectional case control study. *Rev Bras Ginecol Obstet* 2015; **37**:411–416.
48. Ding Y, Xia B, Zhuo G, Zhang C, Leng J. Premature ovarian insufficiency may be associated with the mutations in mitochondrial tRNA genes. *Endocr J* 2019; **66**:81–88.
49. Broekmans FJ, Soules MR, Fauser BC. Ovarian aging: mechanisms and clinical consequences. *Endocr Rev* 2009; **30**:465–493.
50. Tatone C, Amicarelli F, Carbone MC, Monteleone P, Caserta D, Marci R, Artini PG, Piomboni P, Focarelli R. Cellular and molecular aspects of ovarian follicle ageing. *Hum Reprod Update* 2008; **14**:131–142.